Nuclear Instruments and Methods in Physics Research A 632 (2011) 52–58

Contents lists available at ScienceDirect

Nuclear Instruments and Methods in Physics Research A

journal homepage: www.elsevier.com/locate/nima

Analytical solutions for space charge fields in TPC drift volumes

S. Rossegger [a,b,*], B. Schnizer [b], W. Riegler [a]

[a] CERN PH, CH-1211 Geneve 23, Switzerland
[b] Institut für Theoretische Physik—Computational Physics, Technische Unisersität, A-8010 Graz, Austria

ARTICLE INFO

Article history:
Received 7 December 2010
Accepted 27 December 2010
Available online 5 January 2011

Keywords:
Time Projection Chamber
Calibration
Green's function
Space charge

ABSTRACT

At high particle rates and high multiplicities, Time Projection Chambers can suffer from field distortions due to slow moving ions that accumulate within the drift volume. These variations modify the electron trajectory along the drift path, affecting the tracking performance of the detector. In order to calculate the track distortions due to an arbitrary space charge distribution in a TPC, novel representations of the Green's function for a TPC-like geometry were worked out. This analytical approach permits accurate predictions of track distortions due to an arbitrary space charge distribution (by solving the Langevin equation) as well as the possibility to benchmark common numerical methods to calculate such space charge fields.

The basic concept of calculating the trajectory-distortions of charged particles due to space charge effects is shown in Fig. 1. The first step is to calculate the electrical field deviations due to positive ions accumulated within the volume. Up to now, this task is usually performed by solving the Poisson equation with the help of discrete numerical methods like Finite Elements. Due to computational limitations, assumptions like radial symmetry are common. Therefore, non-radially symmetric space charge distribution are difficult to handle within a feasible time and accuracy. Furthermore, due to limitations regarding the cell size of the model, the space charge distribution are generally assumed to be rather smooth. A short description of a common numerical model as it is used within the STAR experiment can be found in Ref. [1]. In contrast to Ref. [1], this paper presents the analytical solution based on Green's functions to calculate the field deviations, for geometries typically used for TPCs (coaxial cavities, see for example Ref. [2]). Further details can be found in Ref. [3] (or Ref. [4] for a slightly different TPC geometry, namely a bi-sected coaxial cavity as proposed for the PANDA experiment [5, p. 115]). Step two in Fig. 1 represents the calculation of the consequent distortions of the electron drift. This can be achieved by solving the Langevin equation as shown in Ref. [6]. For the case of E nearly parallel to B, a simplified integral technique was introduced in Ref. [7] which is valid up to the second order. More detailed algorithms, which solve the drift equation via algorithms like Euler or Runge–Kutta, are built into the program packages like Garfield or Aliroot (see Ref. [8] or Ref. [9]).

More details on the individual steps, the calculation techniques as well an application can be found in Ref. [10].

1. Point charge in a coaxial cavity

The geometry of a typical TPC (see Fig. 2) can be approximated by two concentric cylinders of radii $r=a$ and $r=b$ with $a<b$. The cylinders are closed at $z=0$ and $z=L$. The conductivities of these surfaces bounding a coaxial cylindrical cavity are assumed to be infinite. The task is to calculate the potential and the electric field due to an arbitrary charge distribution contained in this cavity. This can be done with the help of the corresponding Green's function $G(r,\phi,z;r',\phi',z')$, which gives the potential at the point (r,ϕ,z) of a point charge located at the point (r',ϕ',z'). The potential of a charge cloud is obtained by integrating Green's function times the charge distribution over the volume occupied by the charge distribution (see Section 2). Methods to derive Green's function and to express the solution are well described by Refs. [11–13]. Useful representations of the solution for the problem at hand are given in Ref. [14].

For the application to the TPC space charge effect it is necessary to evaluate the potential and the electric field at almost all points of the cavity, including configurations where the point of observation is near to the source point, and both may be near to one of the boundaries. These requirements lead to considerable difficulties: Green's functions for such a cavity can only be represented by infinite series and/or integrals. These series or integrals may become poorly convergent (those for the electric field components even divergent) on and near manifolds, i.e. curves or surfaces, passing through the source point. This unfavorable behavior is not confined to the singular manifold but

* Corresponding author at: CERN PH, CH-1211 Geneve 23, Switzerland.
E-mail address: Stefan.Rossegger@cern.ch (S. Rossegger).

0168-9002/$ - see front matter © 2011 Elsevier B.V. All rights reserved.
doi:10.1016/j.nima.2010.12.213

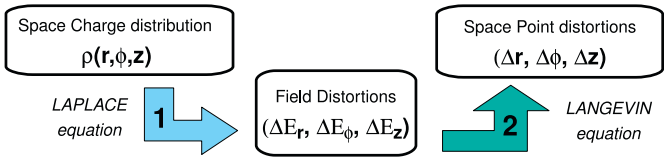

Fig. 1. Basic concept of simulating space charge deviations. Solving the inhomogeneous Laplace equation for a given space charge accumulation ρ leads to the electrical field deviations $\Delta\vec{E}$. Then, by solving the Langevin equation, the resulting electron drift distortions are calculated.

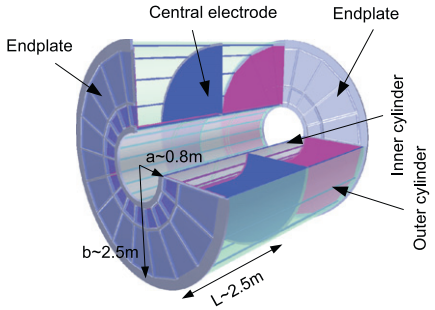

Fig. 2. Schematic representation of the ALICE TPC (dimensions taken from Ref. [2]).

prevails in a volume surrounding it. Fortunately, the same Green's function can be represented in various ways; each representation has its own singular manifold. But these manifolds have different shapes and extents, so one representation may be usable in a volume where another one fails. For that reason it is recommended to find as many different representations as possible and as long as these are practical to use from the point of view of analytical and numerical evaluations.

There are unfavorable configurations where the field and the source point are very near to each other or/and both are very near to a boundary. There are recipes for curing these problems by extracting poorly convergent terms from the series or integrals in such a way that this subtraction can be compensated by known closed expressions. Such remedies were described before Refs. [15,16]. An additional representation using these methods is discussed in Section 1.4.

1.1. Green's function represented by ordinary Bessel functions

The complete expression of Green's function for a coaxial cavity represented by common Bessel functions was derived in Ref. [3] and can be expressed as

$$G(r,\phi,z;r',\phi',z') = \frac{1}{2\pi}\sum_{m=0}^{\infty}\sum_{n=1}^{\infty}(2-\delta_{m0})\cos[m(\phi-\phi')] \times\frac{R_{mn}(r)R_{mn}(r')}{\overline{N}_{mn}^2}\frac{\sinh(\beta_{mn}z_<)\sinh(\beta_{mn}(L-z_>))}{\beta_{mn}\sinh(\beta_{mn}L)} \tag{1}$$

wherein $R_{mn}(r)$, $\overline{N}_{mn}^2$ are given in Eqs. (2), (4) respectively. $z_<$ stands for $0\le z'<z\le L$ and $z_>$ for $0\le z<z'\le L$.

Accounting to the Dirichlet boundary conditions at the inner and outer radii, $r=a$ and $r=b$, we find the following solution for the radial term of the separation ansatz:

$$R_{mn}(r) = Y_m(\beta_{mn}a)J_m(\beta_{mn}r)-J_m(\beta_{mn}a)Y_m(\beta_{mn}r). \tag{2}$$

The expression trivially evaluates to zero for $r=a$. Discrete values of β result from the boundary condition at $r=b$. β_{mn} can be calculated from $x_{mn}=\beta_{mn}b$, which is the n-th zero of

$$J_m(x)Y_m(lx)-J_m(lx)Y_m(x) \quad \text{with } l=a/b. \tag{3}$$

The normalization constant $\overline{N}_{nm}^2$ is

$$\overline{N}_{nm}^2 = \frac{2}{\pi^2\beta_{mn}^2}\left[\frac{J_m^2(\beta_{mn}a)}{J_m^2(\beta_{mn}b)}-1\right]. \tag{4}$$

This is found from a formula for integrals over squares of Bessel functions [17, p. 132, Eq. (11)].

1.2. Green's function represented through modified Bessel functions

The representation of Green's function for a coaxial cylindrical cavity represented through modified Bessel functions is

$$G(r,\phi,z;r',\phi',z') = \frac{1}{\pi L}\sum_{m=0}^{\infty}\sum_{n=1}^{\infty}(2-\delta_{m0})\cos[m(\phi-\phi')]\sin(\beta_n z)\sin(\beta_n z') \times\frac{R_{mn\,1}(r_<)R_{mn\,2}(r_>)}{I_m(\beta_n a)K_m(\beta_n b)-I_m(\beta_n b)K_m(\beta_n a)} \tag{5}$$

with

$$R_{mn\,1}(r) = K_m(\beta_n a)I_m(\beta_n r)-I_m(\beta_n a)K_m(\beta_n r) \tag{6}$$

and

$$R_{mn\,2}(r) = K_m(\beta_n b)I_m(\beta_n r)-I_m(\beta_n b)K_m(\beta_n r). \tag{7}$$

The boundary conditions at the end of the z interval, $\Phi(r,\phi,0)=\Phi(r,\phi,L)=0$ require discrete values for β, namely $\beta_n=n\pi/L$.

A different derivation than described in Ref. [3], which leads to the same solution, can be found in Ref. [14].

1.3. Green's function represented through modified Bessel functions of imaginary order and real argument

The two previous representations of Green's function were based on particular solutions with discontinuous first derivative in z, Eq. (1), or in r, Eq. (5). The existence of a third kind of solution which displays this behavior in ϕ is mentioned in Ref. [18, p. 34].

As derived in Ref. [3], this third kind of a Green's function for a coaxial cavity is

$$G(r,\phi,z;r',\phi',z') = \frac{1}{L}\sum_{k=1}^{\infty}\sum_{n=1}^{\infty}\frac{\cosh[\mu_{nk}(\pi-|\phi-\phi'|)]}{\mu_{nk}\sinh(\pi\mu_{nk})} \times\sin(\beta_n z)\sin(\beta_n z')\frac{R_{nk}(r)R_{nk}(r')}{N_{nk}^2} \tag{8}$$

with

$$R_n(r) = L_{i\mu}(\beta_n a)K_{i\mu}(\beta_n r)-K_{i\mu}(\beta_n a)L_{i\mu}(\beta_n r). \tag{9}$$

The solution is expressed by modified Bessel functions of imaginary order. As discussed in Refs. [19,20], it is favorable for numerical evaluation to use $L_{i\mu}(\beta r)$ instead of $I_{i\mu}(\beta r)$, which is defined by

$$L_{i\mu}(\beta r) := \frac{1}{2}(I_{-i\mu}(\beta r)+I_{i\mu}(\beta r)) \tag{10}$$

as the solutions of the modified Bessel differential equation in radial direction.

By its definition this function fulfills the boundary condition at $r=a$. Since $\beta_n=n\pi/L$ is already discrete from the Dirichlet boundary conditions in z, discrete values of μ must be determined to satisfy the Dirichlet condition at $r=b$. The imaginary value $i\mu_{nk}$ represents the order of the Bessel function, where μ_{nk} is the k-th zero of the following real function of the real variable μ:

$$R_{nk}(\mu_{nk};a,b) = L_{i\mu}(\beta_n a)K_{i\mu}(\beta_n b)-K_{i\mu}(\beta_n a)L_{i\mu}(\beta_n b) = 0. \tag{11}$$

The normalization integrals N_{nk}^2 in Eq. (8) is

$$N_{nk}^2 = \int_a^b [R_n(\mu;r)^2]_{\mu=\mu_{nk}} \frac{dr}{r} \tag{12}$$

are found by numeric integration.

A representation of Green's function equivalent to that given in Eq. (8) may also be derived from the two-dimensional Green's function obtained from Eq. (5) by omitting the dependence on the longitudinal coordinate z through a Watson (or Sommerfeld–Watson) transformation. This is worked out in the appendix of Ref. [3].

1.4. Convergence improvement close to the point charge

All three solutions shown above are hampered by slow convergence properties close to the point charge itself. If combined, they represent however a powerful tool to calculate the resulting potential anywhere but close to the point charge. Several numerical calculations showed that the thickness of the problematic volumes as shown in Fig. 3 decrease rapidly with increasing summation limit. A summation limit of 40 was found to be sufficient to calculate Green's function with sufficient accuracy outside of a volume 0.05 m thick within the ALICE TPC geometry. However, one may need a fast converging solution close to the point charge itself, therefore remedies as proposed in Ref. [15] are used to derive such a representation.

By looking at the Green function represented through ordinary Bessel functions (1) we find the part of the hyperbolic functions to be the decisive term for the convergence.

By expressing the hyperbolic

$$g_0(\beta) = \frac{\sinh(\beta z_<)\sinh(\beta(L-z_>))}{\sinh(\beta L)} \tag{13}$$

in the following form:

$$g_0(\beta) = \frac{e^{-\beta(z_>-z_<)} - e^{-\beta(z_>+z_<)} - e^{-\beta(2L-z_>-z_<)} + e^{-\beta(2L-z_>+z_<)}}{2(1-e^{-2\beta L})} \tag{14}$$

we can identify the problematic terms. The first, second and third exponential in the numerator are responsible for the slow convergence. Directly at the point charge $z=z'$ as well as at the dangerous boundaries in z direction, $z=z'=0$ or $z=z'=L$, this expression would, for increasing β, lead to 1/2. That means within the $z=z'$ plane it cannot contribute to the global converge anymore.

As is shown in Ref. [15], the following method can be used in order to get a better behaved representation. By simply subtracting a term of exponentials this behavior can be cured:

$$\begin{aligned} g_s &= g_0 - \frac{1}{2}[e^{-\beta(z_>-z_<)} - e^{-\beta(z_>+z_<)} - e^{-\beta(2L-z_>-z_<)}] \\ &= \frac{e^{-\beta(2L-z_>+z_<)} + e^{-\beta(2L+z_>-z_<)} - e^{-\beta(2L+z_>+z_<)} - e^{-\beta(4L-z_>-z_<)}}{2(1-e^{-2\beta L})}. \end{aligned} \tag{15}$$

Now, every additional exponential term in Eq. (15) represents a point charge in an infinite double cylinder which can be seen by looking at the limits of the rewritten solution in z direction. For convenience, instead of the boundaries 0 and L we are using h_1 and h_2. For $h_{1,2} \to \pm\infty$ we get

$$\lim_{h_{1,2}\to\infty} \frac{\sinh(\beta(h_1-z_<))\sinh(\beta(h_2-z_>))}{\sinh(\beta(h_1-h_2))} = \frac{1}{2}e^{-\beta(z_>-z_<)} = \frac{1}{2}e^{-\beta|z-z'|}.$$

The expression $\alpha = z_> - z_<$ is independent of its sign since within the term of the point charge in free space it is α^2 and within the correction term it appears within the cosine function, which is symmetric. For that reason we can use $\alpha = z - z'$ instead.

If using g_s instead of g_0 the series is converging rather fast. The correction of these additional terms can be done by using analytical expressions for an infinite (non-closed) coaxial geometry. Such integral representations can be found in Ref. [16]:

$$\begin{aligned} G_C(r,\phi,r',\phi',\alpha) &= G_F(r,\phi,r',\phi',\alpha) + H_C(r,\phi,r',\phi',\alpha) \\ &= \frac{1}{4\pi}\frac{1}{\sqrt{r^2 - 2rr'\cos(\phi-\phi') + r'^2 + \alpha^2}} \\ &\quad - \frac{1}{2\pi^2}\sum_{m=0}^{\infty}\varepsilon_m \cos[m(\phi-\phi')] \\ &\quad \times \int_0^{\infty} d\lambda \cos(\lambda\alpha)[I_m(\lambda r)c_m(\lambda) + K_m(\lambda r)d_m(\lambda)] \end{aligned} \tag{16}$$

with

$$\varepsilon_m = (2-\delta_{m0})$$

$$c_m(\lambda) = K_m(\lambda b)R_m(a,r')/N_m$$

$$d_m(\lambda) = I_m(\lambda a)R_m(r',b)/N_m$$

$$R_m(s,t) = I_m(\lambda s)K_m(\lambda t) - I_m(\lambda t)K_m(\lambda s)$$

$$N_m = I_m(\lambda a)K_m(\lambda b) - I_m(\lambda b)K_m(\lambda a).$$

In Eq. (16), the first term is simply the solution of the potential equation for a unit source in free space. The second term is applying the boundary conditions on the surfaces of the double cylinder geometry. This representation converges as long as both r and r' do not coincide with either the inner or outer radius.

With the help of these converging representations we can rewrite formula (1) with $G_C(r,\phi,r',\phi',\alpha)$ from Eq. (16) and $g_s(\beta)$ from Eq. (15).

$$\begin{aligned} G(r,\phi,z,r',\phi',z') &= G_C(r,\phi,r',\phi',z-z') - G_C(r,\phi,r',\phi',z+z') \\ &\quad - G_C(r,\phi,r',\phi',2L-z-z') + \frac{1}{2\pi}\sum_{m=0}^{\infty}\sum_{n=1}^{\infty}(2-\delta_{m0}) \\ &\quad \times \cos[m(\phi-\phi')]\frac{R_{mn}(r)R_{mn}(r')}{N_{mn}^2}\frac{g_s(\beta_{mn})}{\beta_{mn}}. \end{aligned} \tag{17}$$

The analytic solution (17) is converging fast close to the unit source in every direction but rather slowly close to the cylinder boundaries. This means that in order to improve the convergence close to the point charge itself, the price of slow convergence at the cylinder boundaries must be accepted.

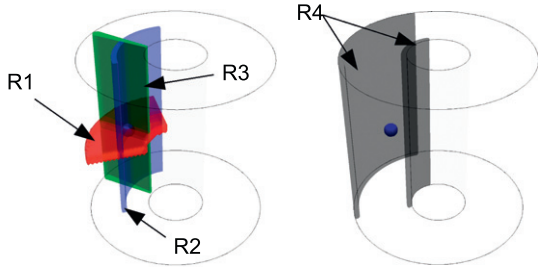

Fig. 3. Problematic regions of Green's functions: R1: $z=z'$, representation through ordinary Bessel functions (1); R2: $r=r'$, representation through modified Bessel functions (5); R3: $\phi=\phi'$, representation through modified Bessel function of imaginary order (8); R4: $r=a$ and $r=b$, representation with improved convergence close to the point charge (17).

1.5. Comparison and regions of fast convergence

All three representations of Green's function which were derived in the previous section are converging rather fast if the point of observation is sufficiently far away from the source point. Basically, all three representations are infinite sums. Each term of such a sum comprises two eigenfunctions with eigenvalues chosen such that they fulfill the Dirichlet boundary conditions. The third factor consists of non-oscillating functions introduced by the method of particular integrals; its first derivative is discontinuous at the manifold where the coordinate of the point of observation coincides with that of the source point. A closer look reveals that just this factor is mainly responsible for the convergence of the infinite sum; but its convergence generating power diminishes as the coordinate of the point of observation approaches that of the source.

In the case of Eq. (1), the eigenfunctions, which have oscillatory character, contribute weakly to the convergence. The singular manifold is the plane $z=z'$. For Eq. (5) we find slow convergence on the cylinder $r=r'$. The third solution (8) shows such a behavior in the plane $\phi=\phi'$. Therefore, by choosing judiciously among the representations of Green's function one can find a representation which converges sufficiently well for all regions of the coaxial cavity except for a neighborhood close to the point charge itself. Thus, methods as discussed in Ref. [15] were used in order to derive Eq. (17), where the region of slow convergence was projected onto the cylindrical boundary. However, the problematic region of slow convergence close to the unit source diminishes when the integration over the charge $\rho(r,\phi,z)$ is performed (see Section 2).

A schematic overview of the dangerous regions with slow convergence is shown in Fig. 3 where all four solutions are compared to each other.

Fig. 4 contains a typical example, a contour plot demonstrating the smooth properties (within the plane $z=z'$) of the innovative representation (8).

Only Green's function (5) is known from the literature [14] which just allowed a convergent representation for the electrical field in the radial direction. The other representation (1) is rather similar as far as the derivation is concerned but it does allow only a convergent representation of the electric field in the longitudinal direction. The third representation derived in Ref. [4] is a novel representation of a Green's function within a coaxial cavity. It renders a convergent infinite sum for the electrical field in the azimuthal direction.

Together, the representations presented in here finally permit the treatment of any space charge distribution within a coaxial cavity, and not only radially symmetrical ones. Combined, they yield convergent series representations for the potential as well as for the electric field in every direction almost everywhere within a coaxial cavity. The following sections contains the fast converging representations for every electrical field component as well as a fast evaluation model which is used for space charge calculations for the ALICE TPC.

The corresponding Green's functions for a rather untypical TPC geometry as that proposed for the PANDA experiment [5, p. 115] require a modification of the boundary conditions in the azimuthal (ϕ) direction. The corresponding Green's functions, plots which display the slow convergence regions as well as certain electrical field plots at chosen representative positions, are given in the appendix of Ref. [4].

1.6. Electric field due to a point charge

The three Green's functions presented in this section can be used to calculate the electric field components. Due to the specific convergence properties of each single representation, a fast converging formula for every electrical field component (E_r, E_ϕ, E_z) can be found via the following derivatives.

1.6.1. Derivative of G in longitudinal (z) direction

Calculating the derivatives of solution (1), which is the representation using ordinary Bessel functions, leads to a converging expression for the field in the longitudinal direction, E_z, but reveals problems in the radial (r) and the azimuthal (ϕ) direction. The converging expression for the derivative in z can be written as

$$\frac{\partial}{\partial z}G(r,\phi,z,r',\phi',z')=\frac{1}{2\pi}\sum_{m=0}^{\infty}\sum_{n=1}^{\infty}(2-\delta_{m0})\cos[m(\phi-\phi')]\frac{R_{mn}(r)R_{mn}(r')}{N_{mn}^2}\times\frac{\partial}{\partial z}\left(\frac{\sinh(\beta_{mn}z_<)\sinh(\beta_{mn}(L-z_>))}{\beta_{mn}\sinh(\beta_{mn}L)}\right) \tag{18}$$

with

$$\frac{\partial}{\partial z}(\sinh(\beta_{mn}z_<)\sinh(\beta_{mn}(L-z_>)))=\begin{cases}\beta_{mn}\cosh(\beta_{mn}z)\sinh(\beta_{mn}(L-z')) & \text{for } 0\le z<z'\le L\\ -\beta_{mn}\cosh(\beta_{mn}(L-z))\sinh(\beta_{mn}z') & \text{for } 0\le z'<z\le L.\end{cases}$$

The (increasing) factor β_{mn} in the numerator would lead to a diverging expression. This divergence is intercepted by the factor β_{mn} in the denominator of the longitudinal term in Eq. (18). Unfortunately, no such compensating factors exist for the radial and azimuthal terms. For example, the additional (increasing) summation indices m in the numerator of the azimuthal cosine expression, which occurs when calculating the derivative in the ϕ direction, destroys the convergence of the sum for the E_ϕ component. For that reason, we use the other representations of

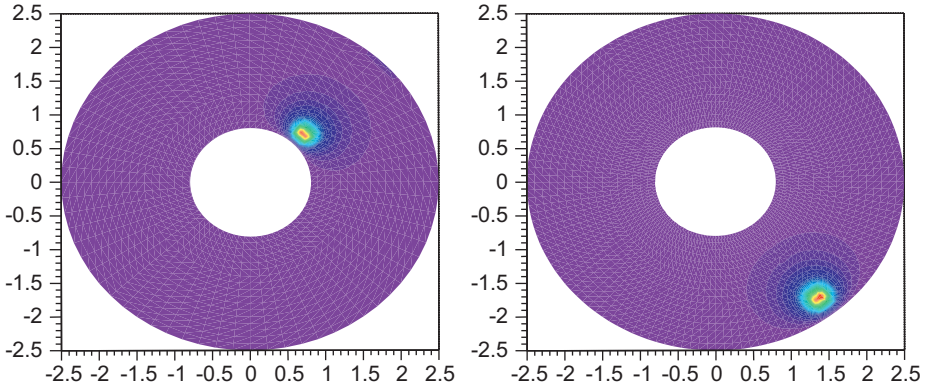

Fig. 4. Potential due to a point charge in the (r,ϕ)−plane plotted with Green's function (8) at $z=z'$; summation limits set to 40; $a=0.8$ m, $b=2.53$ m. Point-charges placed in arbitrary positions.

Green's function to express the electric field components in the radial and the azimuthal direction.

1.6.2. Derivative of G in radial (r) direction

Due to the non-oscillating behavior of the radial term in solution (5), which makes use of modified Bessel function, a non-diverging expression for the field in the radial direction, E_r, can be expressed as shown in the following equation:

$$\frac{\partial}{\partial r}G(r,\phi,z,r',\phi',z') = \frac{1}{\pi L}\sum_{m=0}^{\infty}\sum_{n=1}^{\infty}(2-\delta_{m0})\cos[m(\phi-\phi')]\sin(\beta_n z)\sin(\beta_n z') \times \frac{\partial}{\partial r}\left(\frac{R_{mn\ 1}(r_<)R_{mn\ 2}(r_>)}{I_m(\beta_n a)K_m(\beta_n b)-I_m(\beta_n b)K_m(\beta_n a)}\right) \quad (19)$$

with

$$\frac{\partial}{\partial r}(R_{mn\ 1}(r_<)R_{mn\ 2}(r_>)) = \begin{cases} R'_{mn}(a,r)R_{mn\ 2}(r') & \text{for } a \le r < r' \le b \\ R_{mn\ 1}(r')R'_{mn}(b,r) & \text{for } a \le r' < r \le b \end{cases} \quad (20)$$

wherein $R'_{mn}(s,t)$ is

$$R'_{mn}(s,t) = \frac{\beta_n}{2}(K_m(\beta_n s)(I_{m-1}(\beta_n t)+I_{m+1}(\beta_n t))) + \frac{\beta_n}{2}(I_m(\beta_n s)(K_{m-1}(\beta_n t)+K_{m+1}(\beta_n t)). \quad (21)$$

The attempt to use solution (5) to derive a converging expression for fields in the azimuthal and longitudinal directions fails due to the increasing arguments m and β_n in the first two terms, which are not compensated by any factors in the denominators. The resulting expressions diverge with increasing summation indices.

1.6.3. Derivative of G in azimuthal (ϕ) direction

The third representation as shown in Eq. (8), which uses modified Bessel functions of imaginary order, leads to a converging expression for the electric field in the ϕ direction, whereas the derivatives in radial or longitudinal direction do diverge due to the reasons already mentioned.

$$\frac{\partial}{\partial \phi}G(r,\phi,z,r',\phi',z') = \frac{1}{L}\sum_{k=1}^{\infty}\sum_{n=1}^{\infty}\sin(\beta_n z)\sin(\beta_n z')\frac{R_{nk}(r)R_{nk}(r')}{N_{nk}^2} \times \frac{\partial}{\partial \phi}\left(\frac{\cosh[\mu_{nk}(\pi-|\phi-\phi'|)]}{\mu_{nk}\sinh(\pi\mu_{nk})}\right) \quad (22)$$

with

$$\frac{\partial}{\partial \phi}(\cosh[\mu_{nk}(\pi-|\phi-\phi'|)]) = \begin{cases} -\mu_{nk}\sinh[\mu_{nk}(\pi-(\phi-\phi'))] & \text{for } 0 \le \phi' < \phi \le 2\pi \\ \mu_{nk}\sinh[\mu_{nk}(\pi-(\phi'-\phi))] & \text{for } 0 \le \phi < \phi' \le 2\pi. \end{cases}$$

In summary, each representation of the Green's function derived in Section 1 has its specific application by providing a fast converging expression for one specific electric field component in cylindrical coordinates (E_r,E_ϕ,E_z). Thus, they finally permit the treatment of any truly three-dimensional space charge distribution $\rho(r,\phi,z)$ within a TPC field cage, and not only radially symmetric ones.

2. Electrical field due to an arbitrary space charge distribution

In order to calculate the potential or the electrical field components due to an arbitrary space charge configuration $\rho_c(r',\phi',z')$ we use Green's functions according to

$$\Phi(r,\phi,z) = \frac{1}{\varepsilon_0}\int r'\,dr'\int d\phi'\int dz'\rho_c(r',\phi',z')\cdot G(r,\phi,z,r',\phi',z') \quad (23)$$

wherein ε_0 is the permittivity of free space. The corresponding electrical field components are the corresponding derivatives

$$E(r,\phi,z) = -\nabla\Phi(r,\phi,z) = -\frac{1}{\varepsilon_0}\int r'\,dr'\int d\phi'\int dz'\rho_c(r',\phi',z')\cdot\nabla G(r,\phi,z,r',\phi',z'). \quad (24)$$

2.1. Electric field due to a radially symmetric charge

The field components E_r and E_z due to a charged ring at an arbitrary position (r',z') can simply be calculated via Eq. (18) or (19) by means of skipping the azimuthal summation over m. The summation indices m can be set to zero. The azimuthal field component E_ϕ is anyway zero due to the radial symmetric nature of the problem.

When applying a radial symmetric charge $\rho(r',z')$ within a certain volume $(\Delta r,\Delta z)$, the resulting field configurations can be calculated by integrating over dr and dz.

These solutions can be used to crosscheck the results as obtained via Finite Element methods, which are almost always limited to such two-dimensional (radially symmetric) cases due to computational reasons.

2.2. Electric field due to a constant charge within a voxel

The fields due to a space charge distribution are calculated by multiplying the corresponding charge distribution ρ with Green's function and by integrating over the volume occupied by the charge distribution. When integrating over the complete volume within the coaxial cavity one finds that all three solution, as given in Section 1, comprise rather fast converging expressions for the electric field components. However, when smaller voxels are demanded the specific convergence properties of each solution start to manifest themselves.

In the following we want to calculate the field components due to a constant charge Q within a defined voxel $(\Delta r,\Delta\phi,\Delta z)$ around a center at (r_0,ϕ_0,z_0). We refer to this volume as POC (Piece Of Cake) volume, since it resembles a curved box. The constant charge density $\rho_Q = Q/V$ is used throughout this subsection where V is the volume of the voxel.

The general expression for the potential in such a POC volume is

$$\Phi(r,\phi,z) = \frac{1}{\varepsilon_0}\int_{r_0-\Delta r/2}^{r_0+\Delta r/2} r'\,dr'\int_{\phi_0-\Delta\phi/2}^{\phi_0+\Delta\phi/2}d\phi' \times\int_{z_0-\Delta z/2}^{z_0+\Delta z/2}dz'\rho_Q\cdot G(r,\phi,z,r',\phi',z'). \quad (25)$$

As an example we use Green's function of Eq. (18) which shows good convergence for the calculation of the z-component of the electric field:

$$\begin{aligned} E_z(r,\phi,z,r',\phi',z') &= \frac{1}{\varepsilon_0}\int_{r_0-\Delta r/2}^{r_0+\Delta r/2} r'\,dr'\int_{\phi_0-\Delta\phi/2}^{\phi_0+\Delta\phi/2}d\phi' \times\int_{z_0-\Delta z/2}^{z_0+\Delta z/2}dz'\rho_Q\cdot\frac{\partial}{\partial z}G(r,\phi,z,r',\phi',z') \\ &= \frac{\rho_Q}{2\pi\varepsilon_0}\sum_{m=0}^{\infty}\sum_{n=1}^{\infty}\int_{\phi_0-\Delta\phi/2}^{\phi_0+\Delta\phi/2}d\phi'(2-\delta_{m0})\cos[m(\phi-\phi')] \times\int_{r_0-\Delta r/2}^{r_0+\Delta r/2}r'dr'\frac{R_{mn}(r)R_{mn}(r')}{N_{mn}^2} \times\int_{z_0-\Delta z/2}^{z_0+\Delta z/2}dz'\frac{\partial}{\partial z}\left(\frac{\sinh(\beta_{mn}z_<)\sinh(\beta_{mn}(L-z_>))}{\beta_{mn}\sinh(\beta_{mn}L)}\right). \end{aligned} \quad (26)$$

Here, the integral in the ϕ direction can easily be expressed in analytical form. An analytical expression for the integral in radial direction can be found via hyper-geometric functions ${}_1F_2$ which lead to an expression which is rather unpractical as regards numerical evaluation. Thus it is advisable to use a numerical algorithm for the integration in the radial direction. For the integration in the longitudinal direction, special precautions have to be taken due to the discontinuous properties of the derivative in z. The integration has to be divided into three different regions in z. For these regions, the following analytic expressions for the integral in z can be found. For the sake of simplicity, we write z_L and z_U for the lower and upper integration limits.

$$\int_{z_L}^{z_U} dz' \frac{\partial}{\partial z}\left(\frac{\sinh(\beta_{mn} z_<)\sinh(\beta_{mn}(L-z_>))}{\beta_{mn}\sinh(\beta_{mn}L)}\right)$$

$$= \begin{cases} = \beta_{mn}\cosh(\beta_{mn}z) & \\ \quad \times (\cosh(\beta_{mn}(L-z_L)) - \cosh(\beta_{mn}(L-z_U))) & \text{for } 0 \le z \le z_L \\ = -\cosh(\beta_{mn}(L-z_U))\cosh(z\beta_{mn})\beta_{mn} & \\ \quad + \beta_{mn}(\cosh(\beta_{mn}(L-z))\cosh(z\beta_{mn}) & \\ \quad - \sinh(\beta_{mn}(L-z))\sinh(z\beta_{mn})) & \\ \quad + \beta_{mn}(-\cosh(\beta_{mn}(L-z))\cosh(z\beta_{mn}) & \\ \quad + \sinh(\beta_{mn}(L-z))\sinh(z\beta_{mn})) & \\ \quad - \cosh(\beta_{mn}z_L)\cosh(\beta_{mn}(L-z))(-\beta_{mn}) & \text{for } z_L \le z' \le z_U \\ = -\beta_{mn}\cosh(\beta_{mn}(L-z)) & \\ \quad \times (\cosh(\beta_{mn}z_U) - \cosh(\beta_{mn}z_L)) & \text{for } z_U < z' \le L. \end{cases} \tag{27}$$

The solutions for the field components in the radial and the azimuthal direction (E_r and E_ϕ) can be found via Eqs. (19) and (22). Although the non-oscillating terms which comprise the discontinuity in their derivative allow simple expressions for the integrated term in r and ϕ, special precautions have to be taken as well. When using the analytical expressions for these terms, a procedure similar to that shown in Eq. (27) has to be used.

For example, Fig. 5 shows all three electrical field components as derived from formulas (18), (19) and (22) with a constant charge density $\rho_Q = 1$ within a coaxial cavity (position and dimensions are given in the caption). The fields are plotted in the (r,ϕ)-plane, where their smoothness properties are displayed. The plots were performed with a summation limit of 30.

2.3. Fast evaluation: discretization of the space charge distribution

Although the derived expressions converge rather fast, a numerical evaluation at approximately 7650 points (equal to 10 cm slices within the TPC volume) takes about 2 min of computation time on a common 2.4 GHz stand alone PC. This estimate includes the calculation of all three field components with a summation limit of 30, which is needed to reach an accuracy of 10^{-7}.

In order to improve the calculation time a discretization model was developed which makes use of a pre-calculated look-up table. This look-up table contains a sequence of field values due to constant charges within a POC volume, as described in the previous subsection. For example, one row within this table holds 7650 field values (e.g. the E_r component) at different positions caused by one single POC configuration. The next rows contain the field values due to POC charges at a different position. Therefore, the complete look-up table comprises the sequence of field values due to POC charges at all possible positions within the discretized volume.

Any desired space charge distribution $\rho(r,\phi,z)$ can be discretized with the corresponding sizes of the voxels as they were used to create the look-up table. By doing so, the voxels obtain a weighting parameter which scales the former charge of $\rho_Q = 1$ into the corresponding average charge density within the voxel. Then, the corresponding fields in the look-up table are scaled with the corresponding weighting parameter (charge density within the voxel) which then results in a simple summation of all weighted configurations.

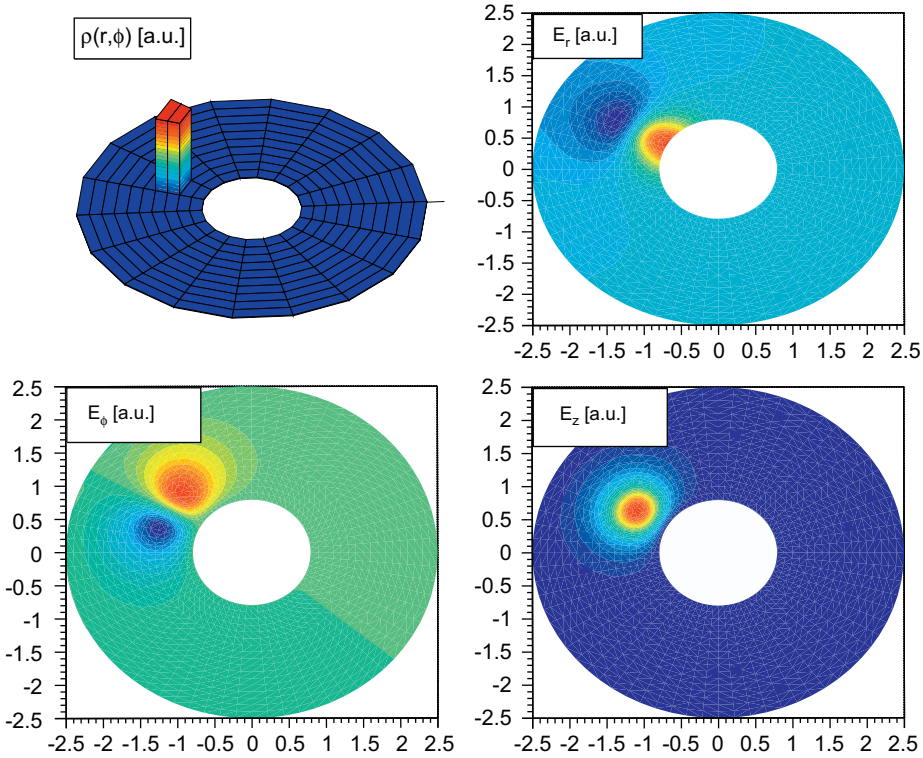

Fig. 5. E field components due to a constant space charge distribution within the region ($1.14 \le r \le 1.48, 2.44 \le \phi \le 2.79, 1.0 \le z \le 1.5$) in the (r,ϕ)-plane at $z=0.8$. General geometry of the cavity: inner radius $a=0.8$, outer radius $b=2.5$, height $h=2.5$.

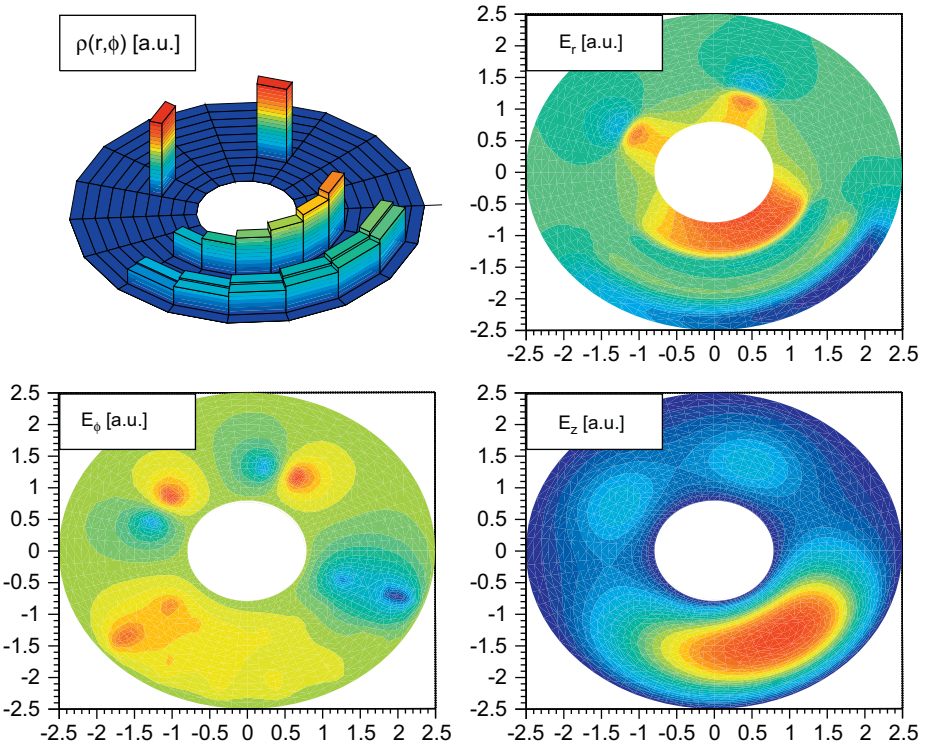

Fig. 6. E field components due to an arbitrary space charge distribution (as shown on the upper left, constant in z) in the (r,ϕ)-plane at $z=0.8$. General geometry of the cavity: inner radius $a=0.8$, outer radius $b=2.5$, height $h=2.5$.

This results in highly accurate values for the field components for a discretized space charge configuration in the TPC volume. Depending on the size of the look-up table this results in a calculation time of less than 1 s for all three field components when a discretization of approximately 10 cm voxels (ALICE TPC geometry) was performed. This discretization size was shown to provide sufficient accuracy for the field values at least for space charge fields with linear dependency in z and a $1/r^2$ dependency in r. When comparing the non-discretized charge distribution (through integration) with the discretization model (10 cm voxels in a look-up table) relative residuals of less than 10^{-6} were observed.

Fig. 6 shows the field components due to an arbitrary chosen charge configuration in a TPC d\rift volume using this "fast evaluation" technique (for details see Ref. [10, Chapter 5]).

3. Summary

We presented a fast converging analytical expressions for Green's function of a TPC geometry i.e. a coaxial cavity bounded on both sides. They can be used to calculate the electric field inhomogeneities due to an arbitrary three-dimensional space charge configurations within a TPC drift volume. For a fast evaluation, a simple discretization approach was discussed. They finally permit an accurate treatment of truly three-dimensional space charge effects as they may occur within the drift volumes of typical TPC geometries.

References

[1] G.V. Buren, et al., Nuclear Instruments and Methods in Physics Research Section A: Accelerators, Spectrometers, Detectors and Associated Equipment 566 (2006) 22 (TIME 2005—Proceedings of the 1st Workshop on Tracking in High Multiplicity Environments).
[2] ALICE TPC Collaboration, Nuclear Instruments and Methods in Physics Research Section A: Accelerators, Spectrometers, Detectors and Associated Equipment 622 (2010) 316. doi:10.1016/j.nima.2010.04.042.
[3] S. Rossegger, Static Green's functions for a coaxial cavity including an innovative representation, CERN-OPEN-2009-003, 2009.
[4] S. Rossegger, Static Green's functions for a bisected coaxial cavity, CERN-OPEN-2009-009, 2009.
[5] The PANDA Collaboration, Technical Progress Report for PANDA 〈http://www-panda.gsi.de/〉, 2009.
[6] W. Blum, W. Riegler, L. Rolandi, Particle Detection with Drift Chambers, second ed., Springer, 2008.
[7] J. Thomas, M. Mager, S. Rossegger, The Langevin equation expanded to 2nd order and comments on using the equation to correct for space point distortions in a TPC, Alice Internal Note, ALICE-INT-2010-016, 2010.
[8] R. Veenhof, Garfield, Version 9, 2010.
[9] ALICE Offline Framework, 〈http://aliceinfo.cern.ch/Offline〉, 2008.
[10] S. Rossegger, Simulation and calibration of the ALICE TPC including innovative space charge calculations., Ph.D. Thesis, CERN-THESIS-2009-124, University of Technology, Graz, 2009.
[11] E.A. Kraut, Fundamentals of Mathematical Physics, McGraw-Hill, New York, NY, 1967.
[12] P.M. Morse, H. Feshbach, Methods of Theoretical Physics. International Series in Pure and Applied Physics, McGraw-Hill, New York, NY, 1953.
[13] B. Schnizer, Analytical Methods in Applied Theoretical Physics. Lecture Notes 〈http://itp.tugraz.at/~schnizer/AnalyticalMethods〉, 2008 (in German, Chapters 12 and 13).
[14] W.R. Smythe, Static and Dynamic Electricity, second ed., McGraw-Hill, New York, NY, 1950.
[15] T. Heubrandtner, B. Schnizer, C. Lippmann, W. Riegler, Nuclear Instruments and Methods in Physics Research Section A 489 (1–3) .
[16] Th. Heubrandtner, B. Schnizer, R. Veenhof. Analytic representations for numeric field computations in the vicinity of a thin wire, 2004, http://consult.cern.ch/writeup/garfield/notes/pointcharge.ps, url=http://consult.cern.ch/writeup/garfield/notes/pointcharge.ps.
[17] G.N. Watson, A Treatise on the Theory of Bessel Functions, second ed., Cambridge University Press, Cambridge, 1966.
[18] H. Buchholz, Elektrische und Magnetische Potential felder, Springer, Berlin, 1957.
[19] F.W.J. Olver, Asymptotics and Special Functions. Computer Science and Applied Mathematics, Academic Press, New York, NY, 1974.
[20] A. Gil, J. Segura, N.M. Temm, Journal of Computational Physics 175 (2002).